IEEE Access
Multidisciplinary | Rapid Review | Open Access Journal

Received February 17, 2021, accepted March 28, 2021, date of publication April 1, 2021, date of current version April 12, 2021.

Digital Object Identifier 10.1109/ACCESS.2021.3070378

Estimation of Path Loss Parameters of a Sub-Terahertz Wireless Channel Using Monostatic Radar

GYE-TAE GIL[1], (Member, IEEE), JU YONG LEE[1], (Member, IEEE), AND DONG-HO CHO[2], (Senior Member, IEEE)

[1]KAIST Institute for Information Technology Convergence, Korea Advanced Institute of Science and Technology (KAIST), Daejeon 34141, South Korea
[2]School of Electrical Engineering, Korea Advanced Institute of Science and Technology (KAIST), Daejeon 305-701, South Korea

Corresponding author: Gye-Tae Gil (gategil@kaist.ac.kr)

This work was supported by Institute for Information & communications Technology Promotion (IITP) grant funded by Ministry of Science and ICT (MSIT) of the Korea Government (No.2018-0-00809, Development on the disruptive technologies for beyond 5G mobile communications employing new resources).

ABSTRACT This paper presents a novel technique for estimating the path loss parameters of radio channels using monostatic radar. To this end, a two-way path loss model for a scenario using monostatic radar for a sub-terahertz (sub-THz) band channel measurement is expressed as a function of a parameter of a one-way path loss model, and then the path loss parameters are estimated using the maximum-likelihood estimation algorithm based on linear regression models, which is based on single reference distance and dual reference distances. To verify the effectiveness of the proposed method, a path loss measurement experiment is conducted in an indoor environment using a frequency modulated continuous wave (FMCW) radar system with the base frequency of 119.5 GHz and the bandwidth of 5 GHz, and then the estimation results based on the proposed method are analyzed.

INDEX TERMS Path loss, channel, sub-THz, monostatic radar.

I. INTRODUCTION

Due to the rapidly increasing wireless communication traffic and the depletion of the existing allocated frequency spectrums, wireless communication researchers are faced with the need to develop a new next-generation communication system that can provide ultrahigh data rates. Among the frequency bands that can solve such a need, the millimeter-wave band from 30 GHz to 300 GHz and the sub-terahertz (sub-THz) band from 0.1 THz to 1 THz are attracting more attention [1]–[6] because the radio frequency (RF) circuits for those bands can be designed and implemented with existing technologies [7].

In designing a new wireless communication system, one of the most important things to consider is to understand the radio channel and the use cases of the system. In particular, to obtain a reliable link budget and signal strength prediction, a path loss model must be established at the beginning stage.

In the literature, there are a few papers on the path loss modeling based on channel measurement campaign of the sub-THz band [8]–[15] mostly using vector network analyzer (VNA) based channel sounder, which can be categorized into D-band (110–170 GHz) [8]–[11] and 300 GHz band measurements [11]–[15]. In case of D-band, [8] presented measurements of indoor D-band short range channels at 110–170 GHz, and analyzed multipath propagation parameters for line-of-sight (LoS), obstructed-LoS, and reflected non-LoS (NLoS) environments; [9] performed wideband directional channel measurements in a shopping mall environment and compared the radio propagation characteristics of 28 and 140 GHz bands in terms of path loss model parameters as well as cluster model parameters; [10] presented indoor wideband propagation measurements and penetration measurements for common materials at 140 GHz.

In case of 300 GHz band, two indoor scenarios (point-to-point link, connection to access point) were investigated in [12], [13] presented experiments on channel modeling at THz band from 260 GHz to 400 GHz for LoS and NLoS scenarios to examine the effect of different distances, angles of arrival and objects acting as reflectors on the achievable capacity; [14] evaluated the performance of a 2×2 multiple input multiple output (MIMO) channel at 298–313 GHz through

The associate editor coordinating the review of this manuscript and approving it for publication was Jie Tang.

simulation based on measurements of four antenna pair channels; In [15], the performance of 300 GHz and 1.25 THz scenarios were evaluated through two-stage measurement-simulation campaign composed of field measurement campaign and ray-tracing assessment, where a THz pulsed imaging and spectroscopy is utilized to measure the scattering properties of typical materials in office rooms. In addition, [11] performed extensive propagation measurements at 30 GHz band, 140 GHz as well as 300 GHz band to compare the path loss parameters of single-frequency and multi-frequency indoor path loss models.

In the case of the existing channel measurement methods, however, expensive equipments, including a VNA, a signal generator, and an optical fiber extension cable, need to be in place to measure the path loss of one-way channels, which becomes an obstacle to exploring new frequency bands for which a transceiver module is not available or hard to implement.

In this paper, we propose an alternative technique that estimates the path loss parameters of a wireless channel using monostatic radar. To this end, a two-way path loss model for a scenario using monostatic radar for sub-THz band channel measurement is expressed as a function of the parameters of a one-way path loss model, and then two methods are presented for estimating channel parameters of the one-way path loss model, one of which is the single reference distance based method and the other is the dual reference distance based method. To verify the effectiveness of the proposed method, we performed a path loss measurement experiment in an indoor wireless environment using a frequency modulated continuous wave (FMCW) radar system with an 122 GHz frequency band, and then we estimated the path loss parameters based on the path loss measurement data.

The remainder of this paper is organized as follows. Section II describes the path loss models for wireless channels. Section III presents two methods for estimating path loss parameters. Section IV presents the experiment and analysis results, and Section V contains the concluding remarks.

Contribution: First, a novel linear regression model is proposed for measuring a channel in a sub-THz band using a monostatic radar. Second, based on the proposed regression model, a maximum-likelihood estimation method for path loss parameters is presented. Third, the effectiveness of the proposed technique is verified through channel measurement campaign in a real indoor environment by using a sub-THz channel measurement system we developed for this work.

II. PATH LOSS MODELS

The path loss models considered in this paper are described as follows.

A. ONE-WAY PATH LOSS MODEL

Fig. 1 shows the configuration of a general communication system of a LoS channel with a propagation distance d. At the transmitting side, the baseband signal is upconverted to the RF band and then transmitted through the transmission antenna, and the signal received at the receiving antenna through the LoS channel is downconverted to the baseband.

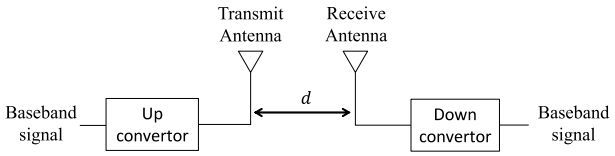

FIGURE 1. Transmission system model in an LoS environment.

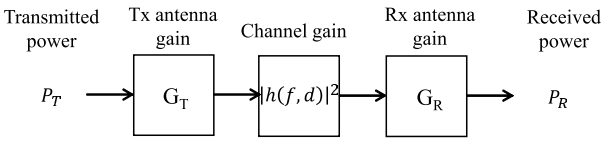

FIGURE 2. One-way path loss model.

Fig. 2 shows the factors that affect the power of the signal in each section of the system with the structure shown in Fig. 1. In the figure, P_T is the power of the transmit signal, G_T and G_R denote the transmit antenna gain and the receive antenna gain, respectively. G_R is the ratio of the effective aperture (A_e) to the aperture of the lossless isotropic antenna (A_{iso}), i.e., $G_R = A_e/A_{iso}$ where $A_{iso} = \frac{\lambda^2}{4\pi}$.

Given P_T, G_T and G_R, the power of the received signal can be expressed as

$$P_R = P_T G_T G_R |h(f,d)|^2 \tag{1}$$

and hence the path loss of the one-way propagation channel becomes

$$PL(f,d) = 10\log_{10}\left(\frac{1}{|h(f,d)|^2}\right).$$

Well-known path loss models for one-way propagation channels include the free-space path model, the close-in (CI) free space reference distance model [4], and the floating-intercept (FI) model [5] defined by the 3rd Generation Partnership Project (3GPP) [16].

In the free space path model, the power of a plane wave arriving at a receiving antenna at a far-field of distance d is written as $p = \frac{P_T G_T}{4\pi d^2} \times L_{abs}(f,d)$, where $\frac{1}{4\pi d^2}$ represents the spreading loss, and $L_{abs}(f,d)$ represents the molecular absorption loss modelled by [17]

$$L_{abs}(f,d) = e^{-k_{abs}(f)d}$$

where $k_{abs}(f)$ is the absorption coefficient.

If we apply the equality of $A_e = G_R A_{iso} = G_R \frac{\lambda^2}{4\pi}$, the power received by the receiving antenna with an effective aperture of A_e is written as

$$\begin{aligned} P_R = pA_e &= \frac{P_T G_T A_e}{4\pi d^2} \times L_{abs}(f,d) \\ &= P_T G_T G_R \times \left(\frac{\lambda}{4\pi d}\right)^2 \times L_{abs}(f,d). \end{aligned} \tag{2}$$

From (1) and (2), the channel gain of the one-way path loss model becomes $|h(f,d)|^2 = \left(\frac{\lambda}{4\pi d}\right)^2 \times L_{abs}(f,d)$, and the path

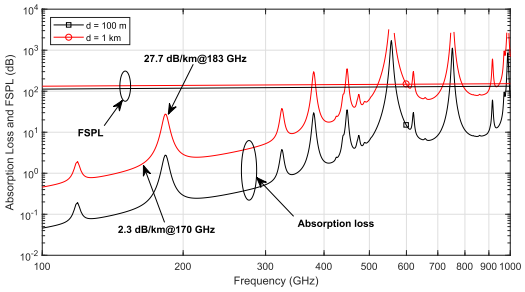

FIGURE 3. Absorption loss and FSPL depending on signal frequency and propagation distance [20].

loss is written as

$$PL^{\mathrm{FS}}(f,d) = FSPL(f,d) + k_{abs}(f)d \times 10\log_{10} e$$

where the first term on the right-hand side represents the free space path loss (FSPL) in a free space without air molecules between the transmitting and receiving antennas, and the second term represents the molecular absorption loss; the FSPL is written as $FSPL(f,d) = 10\log_{10}\left(\frac{4\pi d}{\lambda}\right)^2$.

The CI free space reference distance model, which is a model that considers the effects of self-interferences due to large-scale shadow fading for a propagation distance larger than or equal to the CI reference distance, is defined as [18]

$$PL^{\mathrm{CI}}(f,d) = FSPL(f,d_0) + 10\beta\log_{10}\left(\frac{d}{d_0}\right) + X_\sigma \quad (3)$$

where d_0 denotes the CI reference distance, X_σ represents the measurement noise which is assumed to be a zero-mean Gaussian random variable, and β is the path loss exponent. If we define $I(d)$ to represent the contribution of multi-path fading in the total received signal power, β can be written as (see Appendix A)

$$\beta = 2 - \frac{10\log_{10}\left(1 + \frac{I(d)}{\left(\frac{\lambda}{4\pi d}\right)^2}\right)}{10\log_{10}\left(\frac{d}{d_0}\right)} \quad (4)$$

which indicates that β becomes greater or less than 2 (i.e., $\beta > 2$) at the distance of $d \geq d_0$ depending on whether the multi-path fading is destructive (i.e., $I(d) < 0$) or constructive (i.e., $I(d) > 0$).

The FI model which uses the variable α in the place of $FSPL(f,d_0)$ in (3), is defined as [19]

$$PL^{\mathrm{FI}}(f,d) = \alpha + 10\beta\log_{10}\left(\frac{d}{d_0}\right) + X_\sigma. \quad (5)$$

Note that the effects of molecular absorption are not included in (3) and (5) because the contribution of molecular absorption to the total path loss is negligible compared to that of the FSPL. Fig. 3 shows that the molecular absorption loss per 1 km of transmission / reception distance is about 0.5 dB in the 100 GHz band and about 2.3 dB in the 170 GHz band, which is much smaller than the FSPL exceeding 100 dB. This justifies the exclusion of the molecular absorption term from (3) and (5) when the frequency band of interest is a lower sub-THz band.

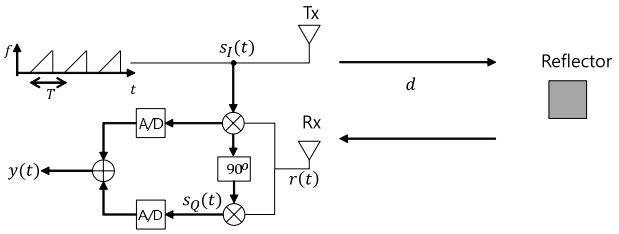

FIGURE 4. Monostatic FMCW radar system model.

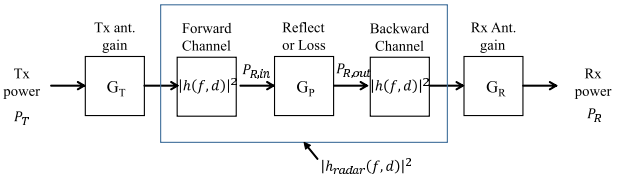

FIGURE 5. Two-way path loss model for a radar system.

According to (3) and (5), the channel gains of the CI free space reference distance model and the FI model are written as

$$\left|h^{\mathrm{CI}}(f,d)\right|^2 = \left(\frac{\lambda}{4\pi d}\right)^2 \left(\frac{d}{d_0}\right)^{-\beta} 10^{-0.1X_\sigma}$$

and

$$\left|h^{\mathrm{FI}}(f,d)\right|^2 = \left(\frac{\lambda}{4\pi d}\right)^2 \left(\frac{d}{d_0}\right)^{-\beta} 10^{-0.1(\alpha+X_\sigma)}$$

respectively. Therefore, completing the CI model means determining the path loss exponent and the variance of the measurement noise, and completing the FI model is identical to determining the path loss exponent, the measurement noise variance, and the parameter α representing the FSPL at the reference distance.

B. TWO-WAY RADAR CHANNEL MODEL

A method of using FMCW radar to estimate the parameters of the one-way path loss model is described as follows.

As shown in Fig. 4, FMCW radar is a technology that can estimate the distance to a reflector, the radial velocity of the reflector, as well as the gain and phase of the propagation channel.

The path loss of the radar channel formed by the radar system and the reflector can be expressed as a two-way path loss model as shown in Fig. 5. In the figure, P_T denotes the power of the transmit signal, and G_T, G_R, G_P denote the transmit antenna gain, receive antenna gain, and the reflector gain, respectively. The power of the signal which arrives at the reflector through the forward path from the transmit antenna to the reflector is written as

$$P_{R,in} = P_T G_T \left|h(f,d)\right|^2$$

and the power of the signal transmitted to a backward path by the reflector is

$$P_{R,out} = P_{R,in} G_P.$$

Then, the power of the signal received by the receive antenna through backward propagation is expressed as

$$P_R = P_{R,out} G_R \left|h(f,d)\right|^2 = P_T G_T G_P G_R \left|h(f,d)\right|^4$$

which means that the path gain of the two-way radar channel is written as

$$\left|h_{radar}(f,d)\right|^2 = G_P \left|h(f,d)\right|^4.$$

Therefore, the total gain of the radar system, defined by $y(f,d)$, is written as

$$\begin{aligned} y(f,d) &= 10\log_{10}\frac{P_R}{P_T} \\ &= 10\log_{10} G_T G_P G_R + 10\log_{10}\left|h(f,d)\right|^4 \\ &= 10\log_{10} G_T G_P G_R - 2\times PL(f,d) \end{aligned} \tag{6}$$

and, using (3) in the place of $PL(f,d)$ in (6), the total gain by the CI model becomes

$$\begin{aligned} y(f,d) &= 10\log_{10} G_T G_P G_R - 20\beta\log_{10}\left(\frac{d}{d_0}\right) \\ &\quad - 2\times FSPL(f,d_0) - 2X_\sigma \\ &= -20\beta\log_{10}\left(\frac{d}{d_0}\right) + \gamma \\ &\quad - 2\times FSPL(f,d_0) - 2X_\sigma \end{aligned} \tag{7}$$

where

$$\gamma = 10\log_{10} G_T G_P G_R.$$

Notice in (7) that β is the proportionality constant of $y(f,d)$ to $\log_{10}\left(\frac{d}{d_0}\right)$ and $\gamma - 2\times FSPL(f,d_0)$ is the bias of $y(f,d)$ at $d = d_0$ when X_σ is assumed to have zero-mean. This implies that β and γ can be estimated with high accuracy if a sufficient number of samples of the total gain $y(f,d)$ are given.

In the FI model, however, the total gain can be expressed from (5) and (6) as

$$y(f,d) = -20\beta\log_{10}\left(\frac{d}{d_0}\right) + \gamma - 2\alpha - 2X_\sigma. \tag{8}$$

in which both γ and α are related to the bias of $y(f,d)$ at $d = d_0$. Therefore, the FI model is not suitable for estimating the path loss parameters with the single frequency measurements unless γ or α is known a priori.

III. ESTIMATION OF PATH LOSS PARAMETERS

Assuming that the total gains measured at N distances using a single frequency radar system are given, methods for estimating the path loss exponent of the CI model and the variance of measurement noise are described as follows.

A. LINEAR REGRESSION MODEL WITH SINGLE REFERENCE DISTANCE

Let f denote the carrier frequency of the radar system, and define $\mathbf{y} = [y(f,d_1), y(f,d_2), \cdots, y(f,d_N)]^T$ as the path loss measurement data corresponding to the N distances in $\{d_i, i = 1,\cdots,N\}$. Then, by writing (7) for all measurements, we get the expression of the path loss at N distances in a vector-matrix form as follows:

$$\begin{aligned} \mathbf{y} = &\begin{bmatrix} -20\log_{10}\left(\frac{d_1}{d_0}\right), & 1 \\ -20\log_{10}\left(\frac{d_2}{d_0}\right), & 1 \\ \vdots & \\ -20\log_{10}\left(\frac{d_N}{d_0}\right), & 1 \end{bmatrix} \begin{bmatrix} \beta \\ \gamma \end{bmatrix} \\ &- 2\times FSPL(f,d_0)\times \mathbf{1}_N - 2\begin{bmatrix} X_{\sigma,1} \\ X_{\sigma,2} \\ \vdots \\ X_{\sigma,N} \end{bmatrix} \end{aligned} \tag{9}$$

where d_0 denotes the single reference distance, $\mathbf{1}_N$ is the N-dimensional vector with all 1's, and $X_{\sigma,1}, X_{\sigma,2}, \cdots, X_{\sigma,N}$ denote the N samples of X_σ.

Define $\mathbf{A}$ as the N-by-2 matrix whose i-th row is $[-20\log_{10}\left(\frac{d_i}{d_0}\right), 1]$, $\mathbf{x} = [\beta,\gamma]^T$, $\mathbf{b} = -2\times FSPL(f,d_0)\times \mathbf{1}_N$ and $\mathbf{w} = -2\times[X_{\sigma,1}, X_{\sigma,2}, \cdots, X_{\sigma,N}]^T$ which is a zero-mean white Gaussian random vector with the covariance matrix of $4\sigma_X^2\mathbf{I}_N$. Then, (9) reduces to

$$\mathbf{y} = \mathbf{A}\mathbf{x} + \mathbf{b} + \mathbf{w}. \tag{10}$$

B. LINEAR REGRESSION MODEL WITH DUAL REFERENCE DISTANCES

One way to reduce the modeling error of a regression model is to segment the total distance ranges into multiple regions by use of two or more reference distances.

Suppose that, given a set of total gain measurements at N distances $\{y(f,d_1), y(f,d_2), \cdots, y(f,d_N)\}$, we want to apply the first reference distance d_{01} and the path loss exponent β_1 for the first $L1$ measurements, and apply the second reference distance d_{02} and the path loss exponent β_2 for the rest.

In this case, by writing (7) for all elements in $\{d_1, d_2, \cdots, d_N\}$, we can formulate the total gain measurements in a vector-matrix form as

$$\mathbf{y} = \mathbf{A}\mathbf{x} + \mathbf{b} + \mathbf{w} \tag{11}$$

where $\mathbf{y} = [y(f,d_1), y(f,d_2), \cdots, y(f,d_N)]^T$, $\mathbf{x} = [\beta_1,\beta_2,\gamma]^T$, $\mathbf{w} = -2\left[X_{\sigma,1}, X_{\sigma,2}, \cdots, X_{\sigma,N}\right]^T$

$$\mathbf{A} = \begin{bmatrix} -20\log_{10}\left(\frac{d_1}{d_{01}}\right), & 0, & 1 \\ & \vdots & \\ -20\log_{10}\left(\frac{d_{L1}}{d_{01}}\right), & 0, & 1 \\ 0, & -20\log_{10}\left(\frac{d_{L1+1}}{d_{02}}\right), & 1 \\ & \vdots & \\ 0, & -20\log_{10}\left(\frac{d_N}{d_{02}}\right), & 1 \end{bmatrix}$$

and

$$\mathbf{b} = -2 \times \begin{bmatrix} FSPL(f, d_{01}) \\ \vdots \\ FSPL(f, d_{01}) \\ FSPL(f, d_{02}) \\ \vdots \\ FSPL(f, d_{02}) \end{bmatrix}.$$

C. MAXIMUM-LIKELIHOOD ESTIMATION

Given the linear regression model in (10) and (11), the maximum-likelihood (ML) estimate for $\mathbf{x}$, which is defined as $\mathbf{x} = [\beta, \gamma]^T$ for the single reference distance model and is also defined as $\mathbf{x} = [\beta_1, \beta_2, \gamma]^T$ for the dual reference distance model, can be derived as follows.

As $\mathbf{w}$ is a zero-mean white Gaussian vector with the covariance matrix of $4\sigma_X^2\mathbf{I}_N$, the likelihood function of $\mathbf{y}$ parameterized by $\mathbf{x}$ is written as

$$p(\mathbf{y}; \mathbf{x}) = \frac{1}{\left(8\pi\sigma_X^2\right)^{N/2}} \exp\left\{-\frac{1}{8\sigma_X^2}\|\mathbf{y} - \mathbf{A}\mathbf{x} - \mathbf{b}\|^2\right\}.$$

Since the likelihood function is maximized at the same value of $\mathbf{x}$ that minimizes $\|\mathbf{y} - \mathbf{A}\mathbf{x} - \mathbf{b}\|^2$, it is straightforward to show that the ML estimate for $\mathbf{x}$ is written as

$$\tilde{\mathbf{x}} = \left(\mathbf{A}^H\mathbf{A}\right)^{-1}\mathbf{A}^H(\mathbf{y} - \mathbf{b}) \tag{12}$$

where $\tilde{\beta} = \tilde{x}(1)$ and $\tilde{\gamma} = \tilde{x}(2)$ in case of the single reference distance model; and $\tilde{\beta}_1 = \tilde{x}(1)$, $\tilde{\beta}_2 = \tilde{x}(2)$ and $\tilde{\gamma} = \tilde{x}(3)$ in case of the dual reference distance model.

D. REMARKS

Some remarks of interest are as follows:

1) The Cramér-Rao lower bound (CRLB) for the vector $\mathbf{x} = [\beta_1, \beta_2, \gamma]^T$ is written as

$$\text{var}\left(\tilde{\mathbf{x}}\right) \geq 8\sigma_X^2 \text{tr}\left\{(\mathbf{A}^H\mathbf{A})^{-1}\right\} \tag{13}$$

where tr{·} represents the trace of a square matrix. *Proof:* Assume that there exists an unbiased estimator $\tilde{\mathbf{x}}$ of $\mathbf{x}$ such that $E[\tilde{\mathbf{x}}] = \mathbf{x}$, and the regularity condition is met. Then, it can be shown that [21]

$$E\left[(\tilde{\mathbf{x}} - \mathbf{x})(\tilde{\mathbf{x}} - \mathbf{x})^H\right] - \mathcal{M}^{-1} \tag{14}$$

is positive semidefinite, where $\mathcal{M}$ is calculated as

$$\mathcal{M} = E\left[\left(\frac{\partial \ln p(\mathbf{y}; \mathbf{x})}{\partial \mathbf{x}^T}\right)^H \frac{\partial \ln p(\mathbf{y}; \mathbf{x})}{\partial \mathbf{x}^T}\right] = \frac{1}{8\sigma_X^2}\mathbf{A}^H\mathbf{A}. \tag{15}$$

Since the trace of a positive semidefinite matrix is non-negative real number, taking the trace of (14), we get

$$E\left[\|\tilde{\mathbf{x}} - \mathbf{x}\|^2\right] - 8\sigma_X^2 \text{tr}\{\left(\mathbf{A}^H\mathbf{A}\right)^{-1}\} \geq 0$$

which can be rewritten as (13). □

2) The ML estimator in (12) is a minimum variance unbiased (MVU) estiamtor for $\mathbf{x}$.

Proof: Using (11) in (12), we have

$$\tilde{\mathbf{x}} = \mathbf{x} + \left(\mathbf{A}^H\mathbf{A}\right)^{-1}\mathbf{A}^H\mathbf{w}. \tag{16}$$

From (16), it can be simply shown tha $\tilde{\mathbf{x}}$ is unbiased (i.e., t $E[\tilde{\mathbf{x}}] = \mathbf{x}$) because $\mathbf{w}$ has zero-mean, and that

$$E\left[(\tilde{\mathbf{x}} - \mathbf{x})(\tilde{\mathbf{x}} - \mathbf{x})^H\right] = 8\sigma_X^2\left(\mathbf{A}^H\mathbf{A}\right)^{-1}$$

because $E[\mathbf{w}\mathbf{w}^H] = 8\sigma_X^2\mathbf{I}$, from which we get

$$E\left[\|\tilde{\mathbf{x}} - \mathbf{x}\|^2\right] = 8\sigma_X^2\text{tr}\{\left(\mathbf{A}^H\mathbf{A}\right)^{-1}\}$$

which means that the ML estimator in (12) achieves the CRLB in (13). □

3) Given an estimate $\tilde{\mathbf{x}}$ and without the knowledge of $\mathbf{x}$, the expected value of $\mathbf{y}$ is written as

$$E[\mathbf{y}] = \mathbf{A}\tilde{\mathbf{x}} + \mathbf{b}. \tag{17}$$

Proof:
Rewriting (11) as $\mathbf{y} = \mathbf{A}\tilde{\mathbf{x}} + \mathbf{A}\left(\mathbf{x} - \tilde{\mathbf{x}}\right) + \mathbf{b} + \mathbf{w}$ and taking expectations on both sides, we get

$$E[\mathbf{y}] = \mathbf{A}\tilde{\mathbf{x}} + \mathbf{b} + \mathbf{A}E\left[\mathbf{x} - \tilde{\mathbf{x}}\right] + E[\mathbf{w}]$$

in which $E\left[\mathbf{x} - \tilde{\mathbf{x}}\right] = \mathbf{0}$ because of the unbiasedness of the ML estimate, and $E[\mathbf{w}] = \mathbf{0}$ because of the zero-mean property of $\mathbf{w}$. □

4) Given an estimate $\tilde{\mathbf{x}}$ and without the knowledge of $\mathbf{x}$, the variance of the measurement error X_σ is estimated by

$$\hat{\sigma}_X^2 = \frac{1}{4N}\left(\mathbf{y} - \mathbf{b} - \mathbf{A}\tilde{\mathbf{x}}\right)^H\left(\mathbf{I} - \mathbf{P}_\mathbf{A}\right)^{-1}\left(\mathbf{y} - \mathbf{b} - \mathbf{A}\tilde{\mathbf{x}}\right). \tag{18}$$

Proof:
From (10) and (11), we have

$$\mathbf{w} = \mathbf{y} - \mathbf{b} - \mathbf{A}\mathbf{x} \tag{19}$$

which can be rewritten using (12) as

$$\mathbf{w} = \mathbf{y} - \mathbf{b} - \mathbf{A}\tilde{\mathbf{x}} + \mathbf{P}_\mathbf{A}\mathbf{w}$$

where $\mathbf{P}_\mathbf{A} = \mathbf{A}\left(\mathbf{A}^H\mathbf{A}\right)^{-1}\mathbf{A}^H$ is the projection matrix of $\mathbf{A}$. Thus, we get

$$\mathbf{w} = \left(\mathbf{I} - \mathbf{P}_\mathbf{A}\right)^{-1}\left(\mathbf{y} - \mathbf{b} - \mathbf{A}\tilde{\mathbf{x}}\right). \tag{20}$$

Define $\hat{\sigma}_w^2$ as the sample variance of an element of $\mathbf{w}$. Then, it satisfies the equality of $\hat{\sigma}_w^2 = 4\hat{\sigma}_X^2 = \frac{1}{N}\mathbf{w}^H\mathbf{w}$, and using (20), it is straightforward to show that the variance of X_σ becomes (18).

□

TABLE 1. FMCW radar sensor specification.

Parameter	Value
Base frequency	119.5 GHz
Bandwidth	5 GHz
Number of chirps	16
Chirp duration	1227 μsec
Output power	-4 dBm
Lens antenna gain	28 dBi
Antenna Aperture angle	$\pm 4^o$

IV. EXPERIMENT AND ANALYSIS

To verify the effectiveness of the two-way path loss model and the dual reference distance based linear regression technique presented in this paper, we conducted an experiment using FMCW radar in an indoor channel environment, and we estimated the path loss parameters based on the measurement data. The venue for indoor channel measurements was on the third floor of KAIST Institute (KI) building in Daejeon, Korea, a five-story building with a large indoor spaces with the width of 11 m and the length of more than 50 m. The space (length $\times$ width $\times$ height) used for this experiement was $11 \times 4 \times 2.7$ m^3 with iron shelves on the left and right sides. The distance from the radar antenna to ceiling was 1.5 m.

A. MEASUREMENT SETUP

Fig. 6 shows the environment where the path loss measurement experiment was performed. In the figure, the white device on the near right side represents the platform on which the FMCW radar is mounted, and the copper plate at the distant center played the role of a reflector that backscatters the radar signal, forming a two-way direct path. In the measurement environment of this experiment, the heights from ground of the radar and the copper plate were equally 1.2 m, the distances of the radar and the copper plate from the iron table were 40 cm, and the minimum distance from the radar to the surrounding scatterers was about 1 m.

Table 1 shows the specification for the FMCW radar used in the measurement experiment [22]. This FMCW radar was manufactured by Silicon Radar GmbH, and the base frequency of the FMCW signal applied in our experiment is 119.5 GHz, the bandwidth is 5 GHz, the number of chirps is 16, and the chirp duration is 1227μsec. The lens antenna installed on the top of a 2×2 planar patch antenna array has the aperture angle of $\pm 4^o$ with the antenna gain of 28 dBi.

The path loss measurement was performed in an indoor LoS environment by collecting the total gains, $\{y(f, d)\}$ for a set of sample distances. Total gains were measured by locating the copper plate to make the distance from the FMCW radar to be 20 cm $\sim$ 4 m at intervals of 10 cm.[1] The measurements were made 10 times at each distance to mitigate the effect of inaccurate path gains measured by the FMCW radar.[2] In addition, to observe the variation of the path loss parameter estimates with the copper plat size and to obtain more accurate estimates, this measurement was performed using copper plates of three difference sizes with widths and heights of 20×20 cm^2, 25×25 cm^2, and 30×30 cm^2.

The control software of the FMCW radar analyzes and reports the information on range, Doppler, radial velocity, azimuth, elevation, and path gain for 15 targets with the highest path gains. In order to identify the direct path record backscattered by the copper plate among the 15 records, a criterion was applied to determine the record with the highest path gain as that of the direct path to the copper plate.

TABLE 2. Measured data for copper plate size: 20×20 cm^2.

Distance, d (m)	Path gain (dB)
0.4	76, 78, 75, 75, 78, 75, 75, 78, 75, 76
0.5	77, 76, 74, 77, 75, 77, 77, 75, 75, 77
0.6	69, 72, 72, 71, 66, 72, 71, 71, 72, 70
0.7	68, 71, 68, 68, 71, 68, 68, 71, 68, 68
0.8	68, 65, 67, 68, 67, 61, 68, 65, 65, 68
0.9	67, 66, 69, 66, 66, 69, 66, 66, 69, 66
1.0	64, 67, 66, 66, 67, 64, 64, 67, 64, 64
1.1	63, 61, 60, 63, 60, 60, 63, 61, 60, 63
1.2	61, 61, 64, 61, 63, 64, 63, 61, 64, 61
1.3	57, 60, 58, 59, 60, 58, 58, 60, 58, 59
1.4	55, 52, 52, 55, 52, 54, 55, 52, 52, 55
1.5	57, 56, 58, 55, 55, 58, 56, 55, 58, 56
1.6	53, 56, 54, 49, 56, 54, 49, 56, 55, 53
1.7	51, 48, 44, 51, 50, 48, 51, 50, 44, 51
1.8	45, 45, 46, 45, 43, 46, 45, 39, 46, 45
1.9	45, 47, 45, 46, 47, 44, 44, 47, 46, 45
2.0	49, 47, 47, 49, 47, 46, 49, 46, 48, 49
2.1	47, 46, 49, 46, 42, 49, 46, 42, 49, 46
2.2	39, 46, 44, 43, 46, 45, 43, 46, 44, 43
2.3	45, 42, 44, 45, 42, 42, 45, 44, 42, 45
2.4	45, 48, 48, 46, 45, 48, 45, 46, 48, 46
2.5	39, 42, 41, 35, 42, 39, 42, 42, 39, 41
2.6	45, 45, 43, 45, 44, 42, 45, 43, 42, 45
2.7	38, 36, 39, 38, 36, 39, 38, 32, 39, 38
2.8	42, 43, 37, 41, 43, 42, 37, 44, 42, 41
2.9	39, 32, 36, 39, 38, 36, 39, 38, 39, 39
3.2	35, 34, 33, 34, 33, 32, 35, 33, 32, 35

B. MEASUREMENT AND ANALYSIS RESULTS

Fig. 7 shows the measured total path gains and the expected values which were analyzed based on the CI model for the cases when the copper plates of three different sizes were used as reflectors. The measured data corresponding to the figures in Fig. 7 are contained in Table 2 to Table 4. Raw Data measured under low signal-to-noise ratio (SNR) conditions

[1]The path loss parameters for line-of-sight channels with a distance of less than 4 m in indoor environments are important parameters that reflect the channel characteristics of indoor point-to-point (P2P) applications.

[2]The primary sources of the long-term variation of the path gain in a fixed experimental environment include random amplitude noise [24] of local oscillator signals and the radar cross section (RCS) drift uncertainty of scatterers [25, p. 5].

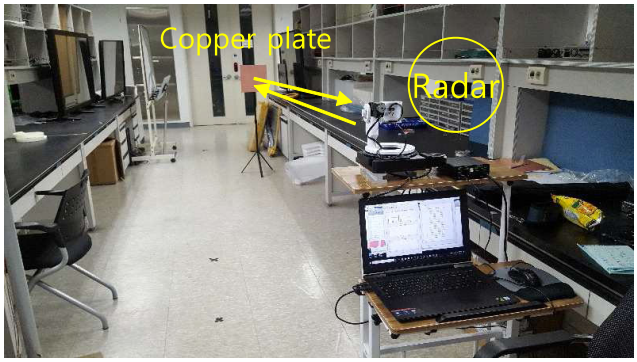

FIGURE 6. Experiment environment.

TABLE 3. Measured data for copper plate size: 25 × 25 cm^2.

Distance, d (m)	Path gain (dB)
0.4	77, 77, 78, 77, 76, 79, 72, 77, 79, 72
0.5	76, 78, 71, 75, 78, 75, 71, 78, 77, 77
0.6	74, 72, 71, 74, 71, 71, 74, 67, 71, 74
0.7	70, 70, 73, 66, 66, 73, 71, 70, 73, 66
0.8	70, 71, 69, 65, 72, 70, 69, 72, 69, 69
0.9	66, 64, 65, 66, 64, 59, 66, 63, 59, 66
1.0	66, 66, 68, 65, 65, 68, 66, 66, 68, 65
1.1	64, 67, 60, 65, 67, 60, 64, 67, 60, 60
1.2	67, 65, 65, 67, 64, 65, 67, 64, 64, 67
1.3	62, 61, 64, 62, 62, 64, 62, 62, 64, 61
1.4	59, 61, 59, 54, 61, 59, 59, 61, 59, 59
1.5	58, 57, 57, 59, 57, 56, 59, 56, 56, 59
1.6	54, 53, 56, 53, 54, 56, 53, 53, 56, 53
1.7	53, 56, 54, 54, 56, 53, 53, 56, 54, 53
1.8	51, 50, 49, 52, 49, 49, 51, 49, 50, 51
1.9	50, 50, 53, 50, 50, 53, 50, 50, 53, 50
2.0	47, 49, 47, 47, 49, 46, 46, 49, 46, 46
2.1	50, 43, 49, 50, 48, 44, 50, 48, 48, 50
2.2	41, 47, 48, 45, 45, 48, 45, 45, 48, 45
2.3	47, 47, 46, 46, 47, 44, 44, 47, 44, 40
2.4	41, 41, 34, 41, 38, 38, 41, 38, 38, 41
2.5	44, 44, 45, 42, 43, 45, 43, 43, 45, 42
2.6	39, 42, 41, 41, 42, 39, 40, 42, 43, 41
2.7	44, 42, 42, 44, 41, 41, 44, 41, 41, 44
2.8	43, 44, 43, 41, 41, 44, 41, 43, 44, 41
2.9	34, 37, 36, 37, 35, 34, 37, 34, 36, 35
3.0	35, 35, 32, 33, 35, 32, 35, 32, 31, 33
3.1	31, 32, 33, 32, 31, 33, 35, 32, 34, 31
3.2	31, 34, 35, 34, 31, 34, 37, 35, 34, 37
3.3	34, 34, 37, 35, 35, 37, 37, 35, 38, 36
3.4	37, 35, 35, 38, 37, 33, 32, 35, 35, 35
3.7	32, 32, 35, 32, 37, 37, 36, 37, 34, 37
3.8	37, 35, 35, 31, 31, 31, 31, 31, 31

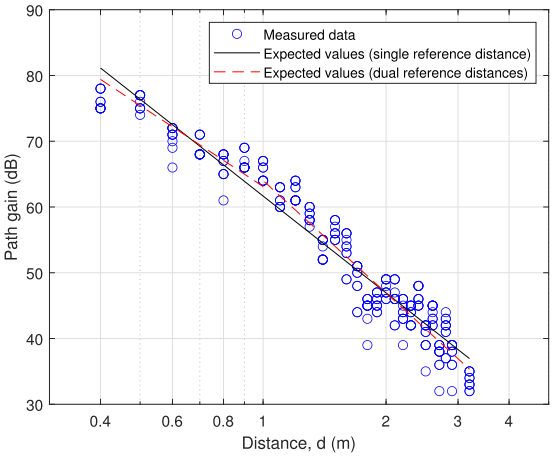

(a) Copper plate size: 20 × 20 cm^2.

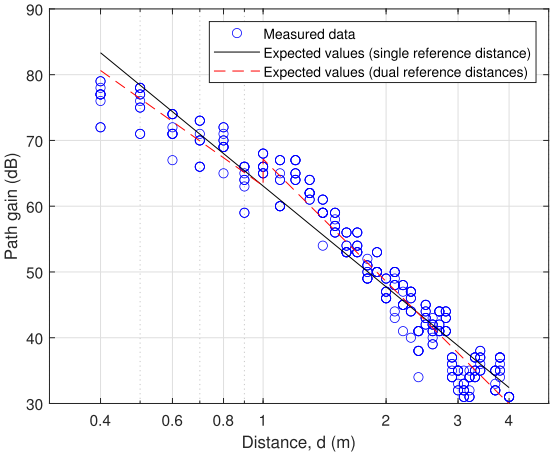

(b) Copper plate size: 25 × 25 cm^2.

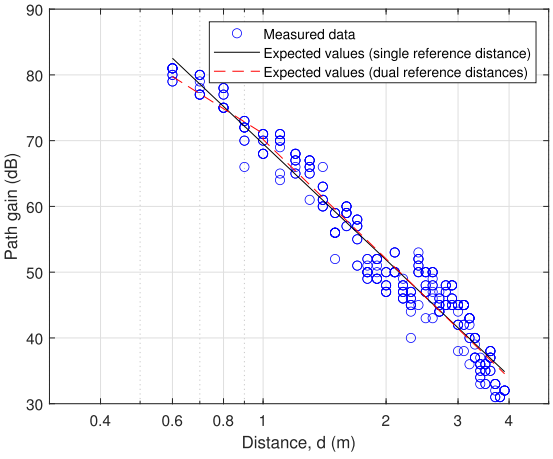

(c) Copper plate size: 30 × 30 cm^2.

FIGURE 7. Measured path gains, and expectation of the path gain estimated based on the CI model.

under 30 dB were invalidated because we cannot guarantee accuracy. In the figure, the circles are the measured total gains of the two-way propagation paths. The solid lines are the expected value of the total path gain for the two-way propagation path that was estimated based on the estimates $\tilde{\beta}$ and $\tilde{\gamma}$ of the CI model. The single reference distance used for the regression model was $d_0 = 10$ cm. The dotted lines show the expected value of the total path gain for the two-way propagation path that was estimated based on the estimates

TABLE 4. Measured data for copper plate size: 30 × 30 cm^2.

Distance, d (m)	Path gain (dB)
0.6	80, 81, 81, 81, 81, 81, 79, 81, 80, 79
0.7	80, 77, 79, 80, 77, 77, 80, 77, 78, 80
0.8	77, 75, 78, 75, 75, 78, 75, 75, 78, 77
0.9	72, 73, 72, 66, 73, 70, 70, 73, 72, 72
1.0	71, 70, 70, 71, 68, 68, 71, 68, 68, 71
1.1	64, 70, 71, 70, 65, 71, 70, 70, 71, 69
1.2	66, 68, 65, 67, 68, 68, 65, 68, 67, 67
1.3	67, 66, 66, 67, 65, 66, 67, 65, 61, 67
1.4	61, 61, 63, 66, 61, 63, 60, 60, 63, 60
1.5	56, 59, 52, 56, 59, 56, 56, 59, 56, 56
1.6	60, 59, 59, 60, 57, 57, 60, 59, 59, 60
1.7	55, 51, 58, 57, 57, 58, 57, 51, 58, 55
1.8	50, 52, 50, 50, 51, 49, 49, 52, 50, 50
1.9	52, 50, 49, 52, 49, 51, 52, 49, 49, 52
2.0	47, 48, 50, 48, 48, 50, 47, 47, 50, 47
2.1	50, 53, 50, 50, 53, 50, 50, 53, 50, 50
2.2	48, 47, 47, 48, 46, 46, 49, 46, 47, 48
2.3	40, 44, 47, 46, 46, 47, 45, 45, 47, 45
2.4	52, 52, 45, 50, 52, 50, 51, 53, 51, 50
2.5	50, 47, 48, 50, 47, 47, 50, 48, 43, 50
2.6	48, 47, 49, 46, 50, 50, 50, 43, 50, 48
2.7	44, 46, 45, 45, 46, 44, 45, 47, 44, 44
2.8	47, 45, 45, 48, 45, 47, 48, 45, 45, 48
2.9	46, 46, 48, 46, 48, 48, 45, 45, 48, 45
3.0	44, 45, 45, 38, 45, 42, 45, 45, 42, 42
3.1	45, 45, 42, 45, 45, 38, 45, 45, 42, 45
3.2	36, 43, 43, 43, 40, 43, 42, 40, 43, 43
3.3	40, 40, 37, 37, 40, 40, 37, 40, 39, 37
3.4	36, 35, 36, 36, 33, 34, 36, 35, 34, 37
3.5	35, 36, 33, 35, 36, 33, 36, 35, 37, 38
3.6	37, 37, 38, 38, 35, 38, 35, 37, 33, 31
3.7	33, 31, 32, 33, 33, 31, 31, 31, 32, 32
3.9	32, 32

$\tilde{\beta}_1$, $\tilde{\beta}_2$ and $\tilde{\gamma}$ of the CI model. The dual reference distances used for the regression model were $d_{01} = 10$ cm and $d_{02} = 1$ m. The expected values were calculated using (17).

It is observed that there are similar patterns in the slope of path gains with the distance in all the figures of Fig. 7. The slope of decrease of path gains is moderate when the distance is below 1 m, but it becomes steep as the distance goes beyond 1 m. The lines for the expected values show that the linear regression based on dual reference distances fits the measurement data better than the linear regression based on single reference distance.

Table 5 and Table 6 show the estimation results of the parameters of the CI model through linear regression using the single reference distance and the dual reference distances, respectively. In the tables, the $\tilde{\gamma}$ estimates have a large value of beyond 200 dB because they include gains generated in the RF chains of the transmitter and the receiver.

The tables reveal that the dual reference distances method has a lower error variance, var (X_σ), compared to the single

TABLE 5. Estimation results based on single reference distance.

Copper plate size (cm^2)	$\tilde{\beta}$	$\tilde{\gamma}$ (dB)	var(X_σ)
20 × 20	2.446	219.0	2.39
25 × 25	2.546	222.4	3.11
30 × 30	2.932	236.6	2.12
Average value	2.641	222.989	2.54

TABLE 6. Estimation results based on dual reference distances.

Copper plate size (cm^2)	$(\tilde{\beta}_1, \tilde{\beta}_2)$	$\tilde{\gamma}$ (dB)	var(X_σ)
20 × 20	(2.045, 2.839)	212.4	1.89
25 × 25	(2.203, 3.090)	215.6	1.97
30 × 30	(1.955, 3.014)	218.6	2.15
Average value	(2.068, 2.981)	215.5	2.00

reference distance method. This means that the dual reference distance based linear regression method has better performance in terms of accuracy than the single reference distance based linear regression method.

The tables also show that the value of $\tilde{\gamma}$ varies with the size of the reflector. This indicates that the reflector gain, G_P, is affected by the size of the reflector used in the experiment because the parameter γ is defined by $\gamma = 10 \log_{10} G_T G_P G_R$ in which G_T and G_R are quasi-static variables.

Moreover, Table 6 shows that the dual reference distances based linear regression method had an average path loss exponent of 2.068 which is very close to that of FSPL when the distance was below 1 m, while it showed an average path loss exponent of 2.981 when the distance was beyond 1 m. Notice that the 1 m distance is the distance from the radar to the first scatterer of our measurement environment. It is understood that the increase in the path loss exponent value at the distance beyond 1 m was caused by the aggregated self-interference due to the multiple scatterers (i.e., iron table, iron shelf, and ground) with diverse relative permittivities (see Apendix B).

V. CONCLUSION

In this paper, we presented a novel method for estimating the path loss parameters of a wireless channel using monostatic radar, and we analyzed the path loss parameters of the one-way propagation channel through linear regression based on the path loss measurements of the 122 GHz frequency band obtained using FMCW radar.

We demonstrated that the path loss exponent estimated using the proposed method based on dual reference distances coincides with that of the FSPL at the distance of below 1 m, which validates the reliability of estimating the path loss parameters using FMCW radar. The path loss exponent was larger than 2.0 at a distance of beyond 1 m, which characterizes the contributions of the scatterers and their reflection properties in the indoor channel environment where the experiment was conducted.

This confirms that the proposed technique using monostatic radar is an effective way to analyze channel characteristics of new frequency bands for next-generation wireless communications.

APPENDIX A
PROOF OF THE EQUATION (4)

The measured value of a path loss is written as

$$PL(f, d) = 10\log_{10}\frac{P_t}{P_r} + X_\sigma \tag{A.1}$$

where X_σ represents the measurement error, and the received signal power for a one-way propagation channel is written as

$$P_r = P_t\left(\frac{\lambda}{4\pi d}\right)^2 + P_t I(d) \tag{A.2}$$

where $I(d)$ represents the contribution of multi-path fading (or shadow fading) due to the presence of surrounding reflectors. We have $I(d) > 0$ when the multi-path fading is constructive and $I(d) < 0$ otherwise.

Using (A.2) in (A.1), we get

$$\begin{aligned} PL(f, d) &= 10\log_{10}\frac{1}{\left(\frac{\lambda}{4\pi d}\right)^2 + I(d)} + X_\sigma \\ &= 10\log_{10}\frac{1}{\left(\frac{\lambda}{4\pi d_0}\right)^2} + 10\log_{10}\left(\frac{d}{d_0}\right)^2 \\ &\quad - 10\log_{10}\left(1 + \frac{I(d)}{\left(\frac{\lambda}{4\pi d}\right)^2}\right) + X_\sigma \\ &= FSPL(f, d_0) + 10\beta\log_{10}\left(\frac{d}{d_0}\right) + X_\sigma \end{aligned}$$

where

$$\beta = 2 - \frac{10\log_{10}\left(1 + I(d)/\left(\frac{\lambda}{4\pi d}\right)^2\right)}{10\log_{10}\left(\frac{d}{d_0}\right)}.$$

APPENDIX B
L-REFLECTION PLANE MODEL

The ground reflection (two-way) model in [18] can be extended for a channel model with L reflection planes as follows.

Let d is the T-R distance, $h_t(i)$ and $h_r(i)$ denote the distances of the transmit and receive antennas from the i-th reflection plane, respectively. Then, the received signal power with the wavelength λ is expressed as

$$|E_{\text{TOT}}|^2 = \left|\frac{E_0 d_0}{d}\right|^2 \left|1 - \sum_{i=1}^{L}\Gamma_i(d)e^{-j\frac{2\pi\Delta_i(d)}{\lambda}}\right|^2 \tag{B.1}$$

where E_0 is the signal strength at $d = d_0$, $\Delta_i(d)$ is the difference between the lengths of the direct path and the reflection path given by

$$\Delta_i(d) = \sqrt{(h_t(i)+h_r(i))^2 + d^2} - \sqrt{(h_t(i) - h_r(i))^2 + d^2}$$

and $\Gamma_i(d)$ is the reflection coefficient of the i-th reflection plane when the T-R distance is d.

For a reflection plane with the relative permittivity of ε_i, the reflection coefficient $\Gamma_i(d)$ is calculated as

$$\Gamma_i(d) = \frac{\sin\theta_i(d) - X_i}{\sin\theta_i(d) + X_i}$$

where

$$\begin{aligned} X_i &= \frac{1}{\varepsilon_i}\sqrt{\varepsilon_i - \cos^2\theta_i(d)} \\ \sin\theta_i(d) &= \frac{h_t(i) + h_r(i)}{\sqrt{(h_t(i) + h_r(i))^2 + d^2}} \\ \cos\theta_i(d) &= \frac{d}{\sqrt{(h_t(i) + h_r(i))^2 + d^2}}. \end{aligned}$$

For $L = 1$, (B.1) reveals that the interference received through the single reflection path, $\Gamma_1(d)e^{-j\frac{2\pi\Delta_1(d)}{\lambda}}$, becomes constructive or destructive with equal probability because λ is sufficiently smaller than $\Delta_1(d)$ at the carrier frequency of 122.5 GHz. However, the inteference phenomenon through L reflection paths with $L > 1$ might not be as simple as the case for $L = 1$ because the aggregated intereference, $\sum_{i=1}^{L}\Gamma_i(d)e^{-j\frac{2\pi\Delta_i(d)}{\lambda}}$, is determined by d, $\{h_t(i)\}$, and $\{h_r(i)\}$ as well as the relative permittivities $\{\varepsilon_i, i = 1, 2, \ldots, L\}$ of the reflection planes.

REFERENCES

[1] Z. Pi and F. Khan, "An introduction to millimeter-wave mobile broadband systems," *IEEE Commun. Mag.*, vol. 49, no. 6, pp. 101–107, Jun. 2011.
[2] K.-C. Huang and Z. Wang, "Terahertz terabit wireless communication," *IEEE Microw. Mag.*, vol. 12, no. 4, pp. 108–116, Jun. 2011.
[3] S. Rangan, T. S. Rappaport, and E. Erkip, "Millimeter-wave cellular wireless networks: Potentials and challenges," *Proc. IEEE*, vol. 102, no. 3, pp. 366–385, Mar. 2014.
[4] I. F. Akyildiz, J. M. Jornet, and C. Han, "Terahertz band: Next frontier for wireless communications," *Phys. Commun.*, vol. 12, pp. 16–32, Sep. 2014.
[5] L. Wei, R. Hu, Y. Qian, and G. Wu, "Key elements to enable millimeter wave communications for 5G wireless systems," *IEEE Wireless Commun.*, vol. 21, no. 6, pp. 136–143, Dec. 2014.
[6] R. Piesiewicz, T. Kleine-Ostmann, N. Krumbholz, D. Mittleman, M. Koch, J. Schoebel, and T. Kurner, "Short-range ultra-broadband terahertz communications: Concepts and perspectives," *IEEE Antennas Propag. Mag.*, vol. 49, no. 6, pp. 24–39, Dec. 2007.
[7] C. Lin and G. Ye Li, "Energy-efficient design of indoor mmWave and sub-THz systems with antenna arrays," *IEEE Trans. Wireless Commun.*, vol. 15, no. 7, pp. 4660–4672, Jul. 2016.
[8] S. Kim, W. T. Khan, A. Zajic, and J. Papapolymerou, "D-band channel measurements and characterization for indoor applications," *IEEE Trans. Antennas Propag.*, vol. 63, no. 7, pp. 3198–3207, Jul. 2015.
[9] S. L. H. Nguyen, J. Jarvelainen, A. Karttunen, K. Haneda, and J. Putkonen, "Comparing radio propagation channels between 28 and 140 GHz bands in a shopping mall," in *Proc. 12th EuCAP*, Apr. 2018, pp. 1–5.
[10] Y. Xing and T. S. Rappaport, "Propagation measurement system and approach at 140 GHz-moving to 6G and above 100 GHz," in *Proc. IEEE Global Commun. Conf.*, Abu Dhabi, United Arab Emirates, Dec. 2018, pp. 1–6.
[11] C.-L. Cheng, S. Kim, and A. Zajic, "Comparison of path loss models for indoor 30 GHz, 140 GHz, and 300 GHz channels," in *Proc. 11th Eur. Conf. Antennas Propag. (EUCAP)*, 2017, pp. 716–720.
[12] S. Priebe, C. Jastrow, M. Jacob, T. Kleine-Ostmann, T. Schrader, and T. Kürner, "Channel and propagation measurements at 300 GHzz," *IEEE Trans. Antennas Propag.*, vol. 59, no. 5, pp. 1688–1698, May 2011.
[13] N. Khalid and O. B. Akan, "Wideband THz communication channel measurements for 5G indoor wireless networks," in *Proc. IEEE Int. Conf. Commun. (ICC)*, Kuala Lumpur, Malaysia, May 2016, pp. 1–6.

[14] N. Khalid and O. B. Akan, "Experimental throughput analysis of low-THz MIMO communication channel in 5G wireless networks," *IEEE Wireless Commun. Lett.*, vol. 5, no. 6, pp. 616–619, Dec. 2016.
[15] V. Petrov, J. Kokkoniemi, D. Moltchanov, J. Lehtomaki, Y. Koucheryavy, and M. Juntti, "Last meter indoor terahertz wireless access: Performance insights and implementation roadmap," *IEEE Commun. Mag.*, vol. 56, no. 6, pp. 158–165, Jun. 2018.
[16] *Spatial Channel Model for Multiple Input Multiple Output (MIMO) Simulations*, document TR 25.996, 3GPP, Sep. 2012.
[17] J. M. Jornet and I. F. Akyildiz, "Channel modeling and capacity analysis for electromagnetic wireless nanonetworks in the terahertz band," *IEEE Trans. Wireless Commun.*, vol. 10, no. 10, pp. 3211–3221, Oct. 2011.
[18] T. S. Rappaport, *Wireless Communications: Principles and Practice*, 2nd ed. Upper Saddle River, NJ, USA: Prentice-Hall, 2001.
[19] A. Zajić, *Mobile-to-Mobile Wireless Channels*. Norwood, MA, USA: Artech House, 2013.
[20] (Sep. 2016). *International Telecommunication Union Recommendation P.676-11*. Accessed: Nov. 20, 2017. [Online]. Available: https://www.itu.int/rec/R-REC-P.676-11- 201609-I
[21] A. van den Bos, "A Cramér-Rao lower bound for complex parameters," *IEEE Trans. Signal Process.*, vol. 42, no. 10, p. 2859, Oct. 1994.
[22] M. Pauli, B. Gottel, S. Scherr, A. Bhutani, S. Ayhan, W. Winkler, and T. Zwick, "Miniaturized millimeter-wave radar sensor for high-accuracy applications," *IEEE Trans. Microw. Theory Techn.*, vol. 65, no. 5, pp. 1707–1715, May 2017.
[23] S. R. GmbH. *User guide SiRad Simple Evaluation Kit*. Accessed: Feb. 2021. [Online]. Available: https://siliconradar.com/datasheets/User_Guide_Simple_V2.3.pdf
[24] M. C. Budge, Jr., and M. P. Burt, "Range correlation effects on phase and amplitude noise," in *Proc. IEEE Southeastern*, Charlotte, NC, USA, Apr. 1993, p. 5.
[25] *IEEE Recommended Practice for Radar Cross-Section Test Procedures*, Standard 1502TM-2007, Sep. 2007.

GYE-TAE GIL (Member, IEEE) received the B.S. degree in electronic communication engineering from Hanyang University, Seoul, South Korea, in 1989, and the M.S. and Ph.D. degrees in electrical engineering from the Korea Advanced Institute of Science and Technology (KAIST), South Korea, in 1992 and 2004, respectively.

Since 1991, he has been with the Research Center of Korea Telecom. In 2013, he joined the KAIST Institute, where he is currently a Research Professor. His research interests include communication signal processing, which includes synchronization, interference cancellation, and adaptive filter design, orbital angular momentum transmission, and massive antenna technologies for cellular mobile communication systems.

JU YONG LEE (Member, IEEE) received the B.S., M.S., and Ph.D. degrees in electrical engineering and computer science from the Korea Advanced Institute of Science and Technology (KAIST), Daejeon, South Korea, in 1995, 1997, and 2003, respectively.

From 2003 to 2006, he was a Senior Researcher with the System Research and Development Team, Network Systems Division, Samsung Electronics. From 2007 to 2008, he was a Postdoctoral Fellow with the University of Toronto, Toronto, ON, Canada. In 2009, he was a Research Professor with Sungkyunkwan University, South Korea. He is currently a Team Leader and a Research Professor with the Communication and Energy Team, KAIST Institute for Information Technology Convergence. His current research interests include future wireless communication networks and wireless power transfer technology.

DONG-HO CHO (Senior Member, IEEE) received the Ph.D. degree in electrical engineering from KAIST, in 1985.

From 1987 to 1997, he was a Professor with the Department of Computer Engineering, Kyung Hee University. Since 1998, he has been a Professor with the School of Electrical Engineering, KAIST. From 2007 to 2011, he was the Director of the Institute for Information Technology Convergence, KAIST. Since 2009, he has been the Director of the KAIST Online Electric Vehicle Project. From 2010 to 2015, he was the Head of The Cho Chun Shik Graduate School for Green Transportation. From 2011 to 2013, he was an IT Convergence Campus (ICC) Vice-President of KAIST. His research interests include mobile communication, online electric vehicle system based on wireless power transfer, and bioinformatics.